View metadata, citation and similar papers at core.ac.uk

brought to you by CORE

provided by Elsevier - Publisher Connector

Biophysical Journal Volume 90 May 2006 3155–3164

Deletion Variants of *Neurospora* Mitochondrial Porin: Electrophysiological and Spectroscopic Analysis

Greg Runke,* Elke Maier,† William A. T. Summers,* Denice C. Bay,* Roland Benz,† and Deborah A. Court*

*Department of Microbiology, University of Manitoba, Winnipeg, Manitoba, R3T 2N2 Canada; and †Lehrstuhl für Biotechnologie, Theodor-Boveri-Institut (Biozentrum) der Universität Würzburg, Am Hubland, D-97074 Germany

ABSTRACT Mitochondrial porins are predicted to traverse the outer membrane as a series of β-strands, but the precise structure of the resulting β-barrel has remained elusive. Toward determining the positions of the membrane-spanning segments, a series of small deletions was introduced into several of the predicted β-strands of the *Neurospora crassa* porin. Overall, three classes of porin variants were identified: i), those producing large, stable pores, indicating deletions likely outside of β-strands; ii), those with minimal pore-forming ability, indicating disruptions in key β-strands or β-turns; and iii), those that formed small unstable pores with a variety of gating and ion-selectivity properties. The latter class presumably results from a subset of proteins that adopt an alternative barrel structure upon the loss of stabilizing residues. Some variants were not sufficiently stable in detergent for structural analysis; circular dichroism spectropolarimetry of those that were did not reveal significant differences in the overall structural composition among the detergent-solubilized porin variants and the wild-type protein. Several of the variants displayed altered tryptophan fluorescence profiles, indicative of differing microenvironments surrounding these residues. Based on these results, modifications to the existing models for porin structure are proposed.

INTRODUCTION

Mitochondrial porins allow the passage of small soluble molecules across the outer membrane of the organelle. Like their bacterial counterparts, mitochondrial porins are predicted to span the lipid bilayer as β-barrels (reviewed in Bay and Court (1)). In artificial ''black lipid'' bilayers, these proteins create pores with characteristic anion-selective, ''open states'' with conductance of ~4 nS. Upon application of voltage on the order of 50 mV, the pores undergo voltage-dependent gating, which switches them to cation-selective, partially closed states with a conductance of ~2 nS. Mitochondrial porins are also known as voltage-dependent anion channels (VDAC) because of these characteristics (reviewed in Benz (2)).

To understand pore formation and the mechanisms of gating and ion selectivity, knowledge of the transmembrane arrangement of porin is required. Numerous approaches have been taken to delineating the organization of the membrane-spanning segments of porin, but these methods have not led to a unified model (reviewed in Bay and Court (1)). Secondary structure prediction (3,4) and this work (Fig. 1), and black lipid bilayer experiments utilizing either single amino-acid variants (5) or biotinylated porins in the presence of streptavidin (6) (Fig. 1 *A*), have led to models of β-barrels formed by between 12 and 16 β-strands (see Fig. 1). In some cases, the predicted barrel contains the amino-terminus of the protein, which likely forms an α-helix (7,8). Data obtained from N-terminal truncation mutants (9,10) and antibody binding experiments (11) do not support a membrane location for this segment of the protein. Most of the β-strands in the N-terminal 100 residues of porin are predicted to reside in similar positions by most of these approaches (2–6,12) (Fig. 1). In contrast, a unified structural model for the C-terminal two-thirds of the protein is not readily delineated from these different data sets (Fig. 1; discussed in Bay and Court (1)).

Direct approaches, such as x-ray crystallography (reviewed in Schulz (13)) and more recently NMR (14,15,16), have provided detailed structural information regarding bacterial porins. Unfortunately, isolated mitochondrial porins lack the intrinsic structural stability of bacterial porins (10,17, our unpublished results), and similar studies have not been possible with the mitochondrial proteins. Nonetheless, the structural features of bacterial porins are useful predictive tools in studies of their mitochondrial counterparts. Bacterial porins span the membrane as an even-number of β-strands, which are separated by tight turns in the periplasmic space and longer loops exposed to the outside of the membrane (13). Individual loops contribute to the functional size and selectivity of the pore (18,19,20,21,22), to the intersubunit interactions in trimeric porins (23), and can act as phage and colicin binding sites (24,25) as reviewed in Achouak et al. (26). These conclusions have been based, in part, on deletion analyses, which are possible because the deletion of external loops does not affect barrel stability (27). Alternatively, removal of all or part of one or more β-strands would prevent the formation of a β-barrel, as has been demonstrated for FepA (18) and FhuA (28).

Similar deletion analysis of mitochondrial porins is possible given the development of systems that allow their efficient expression in *Escherichia coli* and purification by

Submitted August 11, 2005, and accepted for publication January 27, 2006.

This publication is dedicated to the memory of Dr. Gyula Kispal, University of Pecs, Hungary.

Address reprint requests to Deborah A. Court, Dept. of Microbiology, 301 Buller Bldg., University of Manitoba, Winnipeg, MB, R3T 2N2 Canada. Tel.: 204-474-8263; Fax: 204-474-7603; E-mail: Deborah_Court@UManitoba.ca.

© 2006 by the Biophysical Society

0006-3495/06/05/3155/10 $2.00

doi: 10.1529/biophysj.105.072520

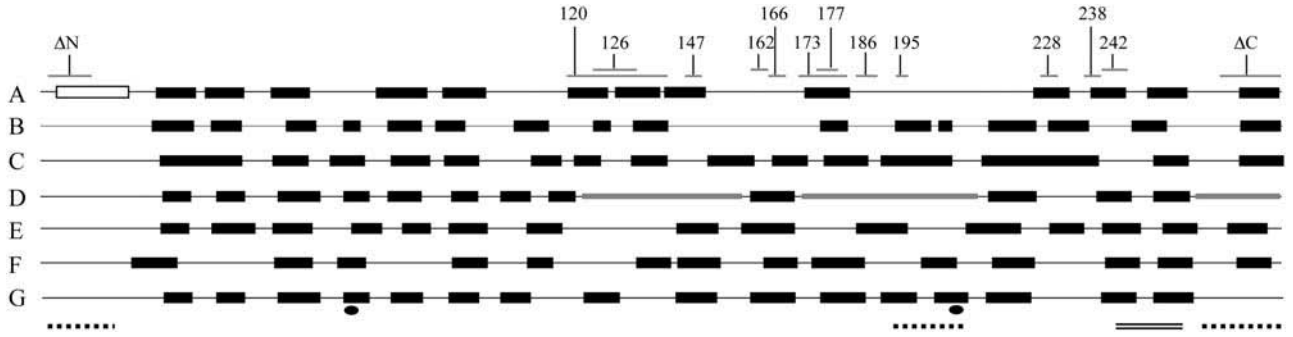

FIGURE 1 Models for the transmembrane arrangement of mitochondrial porin from *Neurospora*. (*A*) 14-strand model of Song et al. (30), based on single amino acid replacement data of (5) and the effects of streptavidin binding to individual biotinylated residues (30,6). (*B*) Sixteen-strand model of Rauch and Moran (3) based on hydropathy and the prediction that β-strands would be interrupted by residues with a high propensity for turn conformation. (*C*) Sixteen-strand model of Benz (2), based on the prediction that a water-filled membrane channel would be formed by β-strands of alternating hydrophobic and hydrophilic residues. (*D*) Sixteen-strand model compiled from the information contained in models *A*, *B*, and *C* (1). Thick gray lines indicate regions for which there were insufficient data to predict topology. (*E*) Sixteen-strand model predicted using a neural network trained on bacterial porins (4). (*F*) Fourteen-strand model obtained using the PRED-TM$\beta\beta$ algorithm ((31), http://bioinformatics.biol.uoa.gr/PRED-TMBB/). (*G*) A revised 16-strand model based on the data presented herein. Black rectangles and thin lines represent predicted β-strands and the intervening regions. The N-terminus is at the left and is predicted to lie in the intermembrane space in models *B*, *C*, *D*, and *G*, and its location is unassigned in *E*. The PRED-TM$\beta\beta$ algorithm (*F*), based on bacterial porins, also places the N-terminus ''inside'' of the outer membrane; i.e., in the periplasmic space. The open rectangle in *A* represents the membrane-embedded α-helix proposed in Song et al. (30). The positions of the subsequent intervening regions alternate between the cytosol and the intermembrane space (see Fig. 4). Thin gray lines above the models represent the regions deleted from the variants, which are labeled with the first position of the deletion. Below the models, the positions of the two Trp residues are indicated by solid circles, and the segments containing epitopes recognized in intact or lysed mitochondria are indicated by solid and dashed lines, respectively (11).

virtue of an N-terminal hexahistidinyl tag (His_6-porin). When reconstituted in nonionic or zwitterionic detergent, fungal ''His-tagged'' mitochondrial porins form pores in artificial bilayers that are indistinguishable from those of the native protein (9,10) and retain ATP binding (29). Initial deletion studies investigated the roles of the carboxyl- and amino-terminal segments of mitochondrial porins from *Neurospora crassa* (9) and *Saccharomyces cerevisiae* (10). Variants of the *Neurospora* protein lacking the N-terminal 12 or 20 residues form flickering, voltage-gated pores with wild-type conductance in the open state (9). The pores formed by a yeast N-terminal deletion variant, lacking only residues 1–8, display a very unstable open state, and exist mainly as ungated channels in low conductance substates (10). A *Neurospora* porin variant lacking the C-terminus, predicted in most models to form a membrane-embedded β-strand, forms a smaller pore that is very stable and retains its gating ability. When both C- and N-terminal segments are absent from this protein, the resulting channels are ungated, cation-selective, with low conductance (9).

Several models for the transmembrane arrangement of *Neurospora* porin are considered in detail in this work and summarized in Fig. 1: those based on secondary structure predictions of Rauch and Moran (3) (Fig. 1 *B*), Benz (2) (Fig. 1 *C*), and Casadio et al. (4) (Fig. 1 *E*), the model developed by Song et al. (30) (Fig. 1 *A*), based on single amino acid replacement data (5) and the effects of streptavidin binding to individual biotinylated residues (30,6), and a composite model based on several experimental and predictive approaches (1) (Fig. 1 *D*). In addition, a model was generated with PRED-TM$\beta\beta$ (Fig. 1 *F*), a new web server trained on outer membrane proteins of gram-negative bacteria, for predicting the topology of β-barrel outer membrane proteins (31). To further probe the models for porin structure, segments of the C-terminal half of the protein were chosen for deletion based on their position in regions of alternating hydrophobic and hydrophilic residues predicted to form β-strands (2), or in large extramembrane loops (4). The pores produced by these variants were subject to electrophysiological analysis, and the folded states of these proteins were probed by circular dichroism (CD) spectrapolarimetry and fluorescence spectroscopy. The latter technique has not been applied to mitochondrial porins, and is very sensitive, allowing investigation of variants that are soluble at low concentrations in detergent.

MATERIALS AND METHODS

Bacterial strains

E. coli strain DH5α (32) was utilized in gene construction; strains XL1-Blue (33) or M15 [pREP4] (34) were utilized for the purification of recombinant porins.

Site-directed mutagenesis

The cDNA encoding *N. crassa* mitochondrial porin (8) was recloned into a pBluescript SK^- vector (Stratagene, La Jolla, CA) for the generation of single-stranded DNA for site-directed mutagenesis using the T7 mutagenesis kit (BioRad, Mississauga, ON, Canada). Mutagenic oligonucleotides obtained from Life Technologies (Burlington, ON, Canada) were used to create different porin deletion variants (Table 1). *Pst*I-*Nar*I fragments containing the modified DNA segments were used to replace the wild-type sequence in the pQE-9 plasmid (9). The sequences of the mutated regions

TABLE 1 Electrophysiological and structural characteristics of porin variants

Porin	Deletion*	Channel conductance (nS)	Voltage gating†	Ion selectivity (pA/pC)	β-Strand content (%)	Fluorescence λ_{max}Trp (nm)	Fluorescence relative intensity
His_6-porin	None	1.5–2.0 4.0–4.5‡	0.54, 0.63‡	1.5‡	29.7	329	1.0
ΔNporin	2–12	0.5–1.5, 4.0‡ (high)§	0.54, 0.60‡	1.2‡	n/c¶	332	1.0
ΔCporin	269–283 (Q)	1.5, 3.0‡ (high)	0.42, 0.50‡	1.3‡	31.6	326	2.1
ΔN/ΔC porin	2–12 and 269–283 (Q)	1, 2.5‡ (high)	0.96, 0.92‡	0.8‡	n/d**	333	1.0
238porin	**N**DRGV	0.5–1.0, 4.0–5.0 (high)	0.63, 0.61	1.7	n/d	n/d	n/d
228porin	**D**PVSF	4.5–5.0 (intermediate)	0.91, 0.91	0.9	25.6	329	1.0
242porin	VAAIAYN (D)	0.5–2.5,4.0 (intermediate)	0.98, 0.92	1.4	31.6	331	0.8
195porin	HKVN	0.5–2.0 (intermediate)§	0.69, 0.93	1.2	n/c	332	0.7
147porin	FLA**G**A	0.5–1.0 (low)§	0.79, 0.86	1.5	29.8	331	0.4
166porin	SAA**V**G (N)	1.0–2.0 (low)	0.75, 0.86††	1.4	n/d	333	0.3
177porin	SAAITA (T)	0.5–1.0 (low)	0.66, 0.59	0.8	n/d	n/d	n/d
186porin	LSVFSA (P)	0.5–1.0 (low)	0.81, 0.88	0.7	n/c	331	0.3
120porin	120–143 (GG)	Insufficient‡‡	n/a‡‡	n/a	28.3	327	1.1
126porin	126–136 (GG)	Insufficient	n/a	n/a	22.9	332	0.6
173porin	173–184 (GG)	Insufficient	n/a	n/a	17.2	337	0.8
162porin§§	ITGY	n/a§§	n/a§§	n/a§§	n/d§§	n/d§§	n/d§§

*Residues absent from the variants are indicated; residues in bold are conserved in porins; residues in parentheses were inserted at the deletion site.
†Values indicate G/G_o at –50 (left value) and +50 (right value) mV.
‡Data taken from Popp et al. (9).
§Relative level of pore formation. High: similar to His_6-porin levels, i.e., >5 pores in first 2 min after pore insertion begins (see Popp et al. (9)). Intermediate: 3–5 pores; low 1–2 pores in first 2 min.
¶Not calculated; CD spectra could not be deconvoluted.
**Not determined; solubility too low for CD or fluorescence analysis.
††At ±30 mV.
‡‡Insufficient pore insertion for determining conductance, voltage gating, or ion selectivity.
‡‡n/a, not applicable, because pore formation was insufficient.
§§Protein cleaved in *E. coli*; not analyzed further.

and flanking DNA to be used in further constructions were confirmed by DNA sequencing at the Institute of Cell Biology, University of Manitoba.

Preparation of porin for biochemical and biophysical analysis

Recombinant His-tagged porin was expressed in *E. coli* and purified from inclusion bodies after solubilization in 8 M urea. The denatured protein was purified by Ni-NTA chromatography, as described (29). When necessary, protein was concentrated in Centricon 10 columns (Amicon, Beverly, MA) to at least 5 μM. Urea was replaced by Genapol X-80 (Fluka, Buchs, Switzerland) through two rounds of dialysis in 1% Genapol X-80, 10 mM potassium phosphate, pH 7. The concentrations of His_6-porin and its variants were determined from their molar extinction coefficients and absorbance at 280 nm.

The purified proteins used for biophysical analysis were diluted 1:10 in 1% Genapol X-80, 1 mM EDTA, 10 mM potassium phosphate, and pH 7 and dialyzed against the same buffer. CD measurements were made on undiluted porin (1–5 μM) in 1% Genapol X-80, 10 mM potassium phosphate, pH 7, within 30 h of initiation of dialysis into Genapol X-80.

Lipid bilayer experiments

The methods used for the ''black'' lipid bilayer experiments have been previously described (9,35). Final protein concentrations in the apparatus were 5–10 ng/ml.

Circular dichroism analysis

CD spectra were obtained using a JASCO (Easton, MD) J-810 spectropolarimeter calibrated with (+)-10-camphorsulfonic acid. Spectra were measured, in a quartz cell with a 0.05-cm path length, at a scan rate of 10 nm/min with a response time of 8 s. CD spectra were corrected by baseline subtraction and were converted to mean residue ellipticity according to the equation: $[\theta]_M = M\theta/\{(10)(l)(c)(n)\}$, where $[\theta]_M$ is 10^{-3} deg cm^2 dmol^{-1}, M is the molecular mass of the porin variant, θ is the measured ellipticity in millidegrees, l is the path length of the cuvette in centimeters (0.05 cm), c is the protein concentration in grams per liter, and n is the number of amino acid residues in the protein. The secondary structures of His_6-porin and the porin variants were determined using the convex constraint algorithm (36) and the membrane-protein reference data set (37). Four pure component curves were used to estimate the fractions of α-helix, transmembrane α-helix (α_T), β-strand, and random coil to generate an ''estimated curve''. To determine the goodness of fit between the experimental CD spectra and the estimated curves, the normalized root mean-square deviation (NRMSD) was calculated using the following equation:

$$\mathrm{NRMSD} = [\Sigma(\theta_{exp} - \theta_{cal})^2/(\Sigma(\theta_{exp})^2]^{1/2},$$

where θ_{exp} and θ_{cal} are the ellipticities of the experimental and estimated CD spectra, respectively. The β-strand content is given in Table 1 only if NRMSD between the estimated and experimental curves was <0.20, at which point the calculated structure cannot be considered to represent the actual structure (38).

Fluorescence analysis

A Shimadzu (Kyoto, Japan) RF-1501 spectrofluorophotometer was used to measure tryptophan fluorescence spectra of porin variants solubilized at 0.4 μM in 1% Genapol-X80. All spectra were measured in a 1-cm

pathlength quartz cuvette after excitation at 296 nm. In most cases, scans were repeated three times and the averaged spectra are presented.

RESULTS

Construction of porin variants

To test the models of porin structure, coding sequences for variants of His_6-porin were created in the pQE-9 vector and expressed in *E. coli*. The regions targeted for deletion reside in different structural elements predicted in each model of porin topology (Table 1, Fig. 1). In principle, deletions in β-strands, or in adjacent sequences needed for folding such as short β-turns, should severely reduce or eliminate the pore-forming ability of the protein. In contrast, removal of sequences in long cytosolic or intermembrane space loops should not prevent pore formation, but might alter other features of the channel, such as ion selectivity or voltage-dependent gating. 162porin could not be studied, as a significant proportion of the protein undergoes proteolytic cleavage in *E. coli* (data not shown).

Electrophysiology of porin variants

Both porin isolated from *Neurospora* mitochondria and His_6-porin expressed in *E. coli* insert into artificial bilayers, causing discrete increases in conductance (9) (see Fig. 2 *A*). For these wild-type proteins, two classes of conductance increase are observed and they reflect the open and partially closed states of the pores; partial closure of a population of pores can be forced by application of applied voltages of $\pm$50 mV (reviewed in Benz (2); see Fig. 2 *B*). Porin lacking 11 N-terminal residues (ΔN2–12porin, referred to as ΔNporin in this work) forms flickering, anion-selective, gated channels. ΔCporin lacks the C-terminal 15 residues (ΔC269–283porin) and the open state of the anion-selective, gated channels it forms is reduced to ~3 nS. The double deletion variant ΔNΔCporin forms small, cation-selective ungated pores (9).

Only two of the porin variants in our study form stable pores with wild-type conductance: 228porin and 238porin (Fig. 2 *A* and Table 1). 238porin is the only variant to produce pores in artificial membranes with similar efficiency to that of wild-type (Fig. 2 *A*). The resulting pores fall into two size classes that are indistinguishable from those of His_6-porin. Thus, residues 238–242 do not contribute directly to the barrel structure of the pore and are most likely part of an extramembrane segment. The large (4–5 nS) 228porin channels are ungated (Fig. 2 *B*). These pores show a slight preference for cations (pA/pC = 0.9) versus the preference for anions (1.3–1.5) of the wild-type pores. 242porin and 195porin form small, anion-selective pores with moderate efficiency. Only the 195porin channels are partially sensitive to voltage-dependent gating (Fig. 2). The anion-selective 242porin channels are of two size classes (Table 1). These channels are not responsive to voltage, suggesting that this variant inserts in two unique conformations, rather than existing in a single structure that can be converted between open and closed states.

Most of the remaining porin variants (Table 1) have limited pore-forming ability, and generally form small, ungated pores that display rapid flickering among different conductance states (Table 1, Fig. 2 *A*). The segments corresponding to the deleted regions therefore likely participate in β-strand or β-turn formation, and their absence would lead to alternative secondary and perhaps tertiary interactions.

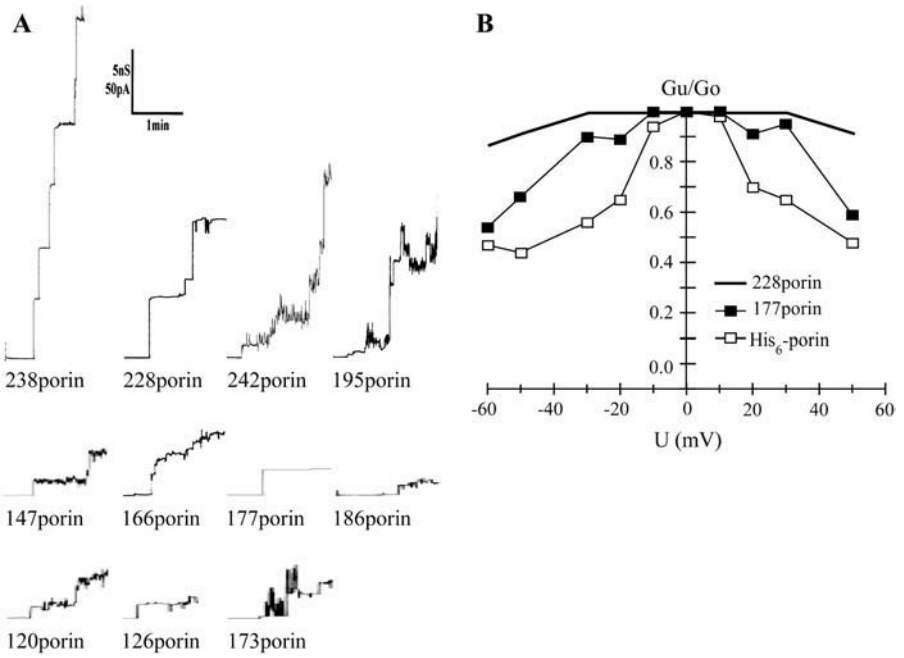

FIGURE 2 Electrophysiology of porin deletion variants. (*A*) Single-channel recordings porin variants in 1% Genapol X-80 was measured as described in Materials and Methods. Two-minute traces are shown, using the scale indicated above 228 porin. (*B*) Voltage-dependent gating of His_6-porin, 177porin and 228porin. The ratio of the conductance, G_u, at voltage U, divided by G_o, is shown as a function of voltage. Data for His_6-porin are replotted from Popp et al. (9).

147porin and 166porin produce small anion-selective pores. The lack of voltage-induced gating in these variants further supports large-scale rearrangements in the folded state of the protein. The net charges of these variants are unchanged from that of His_6-porin, suggesting a significant change in the set of residues lining the channel. 177porin and 186porin both form small, cation-selective pores, although only the former variant displays voltage-dependent gating. The corresponding deletions involve uncharged residues, suggesting that new segments harboring negatively charged residue(s) are placed in the membrane.

Pore formation by 120porin, 126porin, and 173porin was insufficient for further characterization. These variants harbor deletions that encompass the large cytosolic loops proposed by Casadio et al. (4) (Fig. 1 *E*), suggesting that some of the residues in the regions 120–143 and 173–184 are involved in transmembrane β-strand formation.

Detergent-promoted folded state of porin variants

The weak pore-forming ability of several of the variants described above could result from large-scale misfolding of the protein, or from minor disruptions to the folded state that interfere with insertion into the black lipid bilayers. In principle, deletions of short segments of porin might cause localized disruption in secondary structure, and might not alter the overall structural composition of the detergent-solubilized protein, as detected by CD. However, these small, localized perturbations of secondary structure could influence tertiary interactions and therefore the microenvironments of single residues, such as the two tryptophans (W-71 and W-209) in the wild-type sequence; Fig. 1). Such changes can be detected as alterations in the tryptophan (Trp) fluorescence profiles of the proteins. Large deletions, or those involving residues critical for maintaining long-range folding interactions, might be expected to reduce overall β-strand content, in addition to influencing Trp fluorescence. CD and fluorescence measurements were carried out in Genapol-X80 to allow direct comparison with the electrophysiological data.

The CD spectrum produced by wild-type His_6-porin has an overall β-strand character, with a single minimum near 215 nm (Fig. 3 *A*) (10,29). The CD spectra of some of the porin variants resemble that of the wild-type, with a broad minimum near 215 nm (for example, ΔCporin; Fig. 3 *A*). Deconvolution of these spectra revealed β-strand content of ~30% for His_6-porin and three of the variants capable of forming large pores, namely 228porin, 242porin, and ΔCporin (Table 1). All of these variants harbor relatively small deletions (5–15 aa), and the absence of short structural elements not essential for overall folding of the protein would not influence the secondary structure content as determined by CD.

β-strand content is also unchanged in several of the porin variants with severely reduced pore-forming ability. A variant with a large deletion, 126porin, shows a reduction in β-strand content to 23%. 120porin, which harbors a larger deletion flanking that in 126porin, has β-strand content similar to that of His_6-porin. In contrast, 177porin is not sufficiently soluble in Genapol X-80 for CD analysis, whereas the variant with the larger deletion, 173porin, is soluble, but shows significantly reduced β-strand content (17%).

CD spectra suitable for deconvolution could not be obtained for the remainder of the variants (see Fig. 3 *A* for examples, and data not shown), although they were all able to form pores in artificial bilayers. The resulting spectra were either featureless (166porin (Fig. 3 *A*), 177porin, 238porin, and ΔNΔCporin) or the error in the deconvolution of the spectra was too high (ΔNporin (Fig. 3 *A*), 186porin, 195porin). The spectrum of ΔNporin has the general characteristics of that of an α-helical rich protein, namely minima near 208 and 220 nm (Fig. 3 *A*), but could not be reliably deconvoluted using the convex constraint algorithm or other algorithms available through Dicroweb (http://www.cryst.bbk.ac.uk/cdweb/html/home.html). In general, these proteins were poorly soluble in Genapol-X80 (<2–3 μM), whereas His_6-porin was stable at 5–7 μM. CD spectra can be obtained from His_6-porin at low concentrations (1.5 μM; data not shown), indicating that these results reflect poor folding and/or aggregation of variants, rather than the low concentrations of protein.

Fluorescence can provide information regarding the environment surrounding the Trp residues in the protein. Excitation of wild-type His_6-porin produces a fluorescence

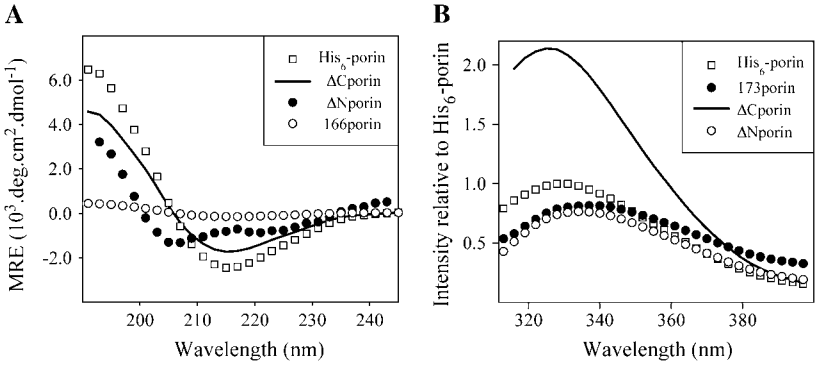

FIGURE 3 Analysis of the folded state of porin variants solubilized in 1% Genapol-X80. (*A*) Circular dichroism spectra obtained from His^6-porin (6.9 μM), ΔCporin (9.8 μM), 166porin (2.4 μM), and ΔNporin (1.6 μM). (*B*) Fluorescence spectra obtained after excitation at 296 nm of 0.4 μM samples of His^6-porin, 173porin, ΔNporin, and ΔCporin.

spectrum with a maximum (λ_{max}Trp) near 329 nm (Fig. 3 *B*), indicating that at least one, and likely both Trp residues (W-71 and W-209), reside in nonpolar environments in the detergent-solubilized protein (Class I fluorescence) (39). The fluorescence maxima for most of the porin variants were within 3 nm of this value, indicating that the β-strands harboring W-71 and W-209 remain in relatively hydrophobic environments in these variants. The exception is 173porin, for which λ_{max}Trp is shifted toward the red (337 nm; Fig. 3 *B*), indicating that at least one of the tryptophans is partially exposed to the aqueous solvent (Class II fluorescence) (39).

The intensity of fluorescence can be quenched by residues, such as aspartate, glutamate, histidine, or phenylalanine, in the vicinity of the tryptophans (40). λ_{max}Trp is unchanged, but the relative emission level is significantly reduced in 126porin, 147porin, 166porin, and 186porin (Table 1), suggesting that the folded states of these variants places at least one of the Trp residues in closer proximity to a quenching residue in the protein or in the detergent micelle. The relative intensities of the fluorescence spectra of the larger internal deletion variants, 120porin, 126porin, and 173porin (Fig. 3 *B*) were the most different from that of His_6-porin (Table 1), as expected for variants that undergo greater changes in overall conformation. The Trp fluorescence spectrum of 126porin indicates that, as for 195porin, the overall hydrophobicity of W-71 and W-209 is unchanged, but that at least one of these residues was placed in closer proximity to quenching groups either in the protein or in the detergent micelle.

ΔCporin is the only variant with increased Trp fluorescence (Fig. 3 *B*). The conformation of ΔNporin is insensitive to the presence of the C-terminal domain, because λ_{max}Trp of ΔNΔCporin (333 nm) was similar to that of ΔNporin (332 nm; Fig. 3 *B*), both of which are slightly red-shifted compared to His_6-porin (329 nm) and ΔCporin, which is slightly blue-shifted (326 nm). 238porin and 177porin produced flat fluorescence spectra with very low intensity (data not shown), suggesting that these proteins may exist mainly as soluble aggregates in detergent. Overall, the fluorescence and CD data support the electrophysiological analysis in demonstrating the formation of alternative β-rich conformations, only some of which are competent for membrane insertion.

DISCUSSION

Predicting the transmembrane arrangement of *Neurospora* porin

Revisions to the model for the transmembrane arrangement of *Neurospora* mitochondrial porin were based on the data presented herein and the experimental data and structural predictions from others. Several assumptions were used to make these predictions. First, it was assumed that the variants with limited pore-forming ability lack at least part of a region normally in a β-strand of β-turn conformation that contributes to channel formation. However, other regions of the protein likely make significant contributions to folding. Second, the assignment of strands based on the effects of single residue replacements on ion selectivity of yeast VDAC1 (5) is based on the assumption that residues contributing to ion selectivity line the barrel, but residues in exposed loops or turns could also influence ion selectivity. Finally, the biotinylation data of Song et al. were used to predict the relative position of particular residues across the membrane, but flexible protein segments could complicate interpretation of these results (6). Finally, rupture of the outer membrane as carried out in antibody-binding studies may alter the membrane to expose portions of the protein normally embedded in the bilayer (11,6). The other consideration in model building was that the five proline residues in porin could not be included in β-strands because these residues disrupt secondary structure (3). From these diverse data sets, a 16 β-strand model can be predicted (Fig. 4).

The N-terminus, including the α-helical region, was placed in the intermembrane space (IMS); deletion of this segment does not prevent pore formation in artificial bilayers (9,10). Furthermore, addition of a His_6-tag to the N-terminus of *Neurospora* porin (41) or a green fluorescent protein to the N-terminus of mouse VDAC1 (42) does not prevent assembly of the protein into the mitochondrial outer membrane. The IMS location for the N-terminus is further supported by antibody-binding data (11,43) (Fig. 1), and by biotinylation studies suggesting that the N-terminus is flexible and not membrane bound (6). D-15 and D-19 contribute to ion selectivity in yeast porin (5); placement of the N-terminus in the IMS suggests that this flexible segment interacts with the barrel structure. Mannella (44) evoked a flexible N-terminus in a model for voltage gating to accommodate the ion selectivity data (5) and cryoelectron microscopy images (45) that suggested an extramembrane location for the N-terminus. In this model, the N-terminus acts as a voltage-sensor that is involved in large-scale structural changes accompanying partial closure of the pore.

Predicted β-strands 1–7 (Fig. 4) were not experimentally tested in this study, and their positions are unchanged from those presented previously (1). In short, this arrangement takes into account the biotinylation studies of Song et al. (6), which places residues N-38, T-69, and K-112 on one side of the membrane, and S-7, H-23, T-53, and A-79 on the other. The exact positions of the β-strands were estimated based on secondary structure predictions of Rauch and Moran (3), Benz (2), and Mannella et al. (12) as discussed (1). Strands of eight residues were arbitrarily chosen; for bacterial porins, the minimum length required to span the lipid bilayer is six residues (46). A longer β-strand from N-75 to A-87 was predicted by the Gibbs sampler (12); all of β5 (L-80 to A-87) is included in this region. β-strands β2, β3, β5, and β6 contain residues that contribute to ion selectivity (5) (Fig. 4) and β4 contains W-71, which resides in a hydrophobic environment in the detergent-solubilized protein (Table 1), suggesting that it is not in an exposed part of the protein.

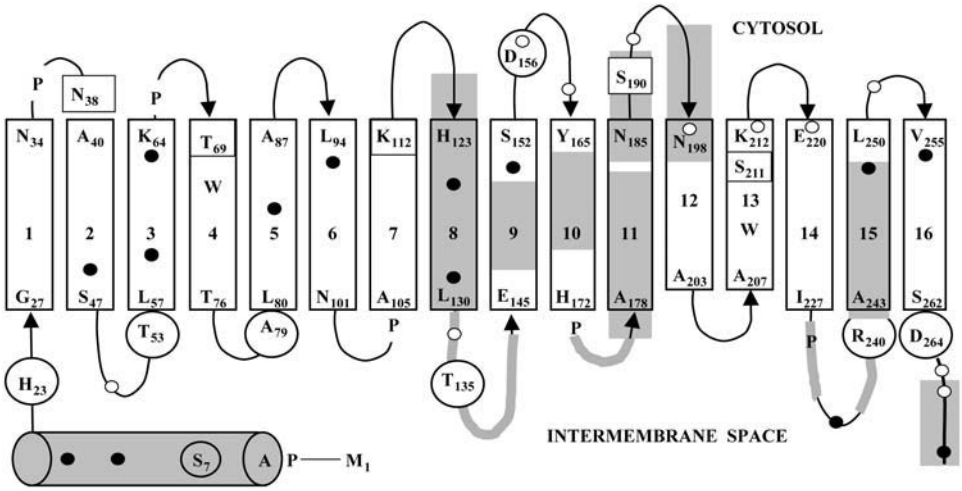

FIGURE 4 Revised model of *Neurospora* mitochondrial porin. The revised 16-strand model is presented, along with sites of deletions (this study and (9)) and single residue variants (5,30) used to generate the model. β-strands are indicated by rectangles; the residues at the ends of the predicted β-strand are indicated by numbers. These positions are estimates, because precise information regarding the residues comprising the β-strands is not available. The intervening loops and turns are thin lines and the predicted N-terminal α-helix are indicated by the cylinder in the lower half of the diagram, which represents the intermembrane space. Circles and squares surround residues predicted by Song et al. (30) to lie on the cytosolic and intermembrane space sides of the membrane. Small solid and open circles indicate residues shown by Blachly-Dyson et al. (5) that either influence or do not influence the ion selectivity of the pore. Deletions created in this study and Popp et al. (9) are shown by shaded regions. For the pairs of nested deletions, 120porin/126porin and 173porin/177porin, only the larger deletion is shown. The single letter code for amino acids is used throughout.

β-strands β3, β4, β6, and β7 are also supported by PRED-TM$\beta\beta$ analysis, whereas β2 and β5 are not. An arrangement lacking β2 and β5 would maintain an even number of β-strands, but it would place H-23 and T-53 on opposite sides of the membrane.

The positions of strands β8–β16 were modified from previous predictions based on the characteristics of the deletion variants. β8 (H-123 to L-130) partially overlaps β-strand predicted by Benz (2) and Rauch and Moran (3). β8 was shifted to include R-125 and R-129 that influence ion selectivity and exclude K-132 that does not (5). Its presence also maintains the relative orientations of K-112 and T-135 (6). In contrast, a large extramembrane loop was predicted in this region by Casadio et al. (4) (S-120 to H-144; Fig. 1 *E*). The deletions in 120porin and 126porin were created to test this prediction. These variants were engineered with two glycyl residues at the junction of the deletions to compensate for the lack of flexibility that may arise if all of the residues separating two β-strands are deleted. The very limited pore formation by 126porin and 120porin suggests that β-strands are disrupted in this variant.

147porin does not form pores, suggesting that β9 includes some or all of residues 147–151. β9 (E-145 to S-152) places D-156 outside the membrane where it would not contribute to ion selectivity, and D-152 in the membrane (5). However, D-156 is likely on the same side of the membrane as T-135, suggesting its placement in the IMS (6). To reconcile these data, a long loop in the IMS that spans T-135 to D-156 could be introduced and the assumption made that only D-152 interacts with the channel in a way that regulates ion selectivity. However, this arrangement would leave only residues 157–164 to create a short β-strand and a loop to connect to β10 (see below). Therefore, D-156 is placed in a loop in the current model, where it could be accessible from the IMS.

A β-strand in the position of β10 (Y-165 to H-172) is predicted by all algorithms, except that of Rauch and Moran (3) (Fig. 1) and is supported by the limited pore formation of 162porin. β10 has been placed to expose R-164 to the cytosol, as this residue is not involved in ion selectivity, and to position P-174 outside of the β-strand. The experimental support for β11 (A-178 to N-185) is the limited pore formation by the nested deletion variants 173porin and 177porin. The deletion in 173porin is predicted to disrupt β11 and the turn between β10 and β11 (Fig. 4), and this variant also has a significantly increased level of random sequence, which likely contributes to its inability to form pores. This region contains a predicted β-strand that is proposed by all models except that of Casadio et al. (4). In the current transmembrane arrangement, β11 is also needed to maintain S-190 on the same side of the membrane as N-38, T-69, and K-112.

The next two β-strands are supported by the lack of pore formation by 195porin, and the likelihood that W-209 resides in a hydrophobic environment. The two strands must arrange S-190 and S-211 on the same side of the membrane, and keep N-198 (E-198 in yeast) and K-212 in positions where they do not participate in ion selectivity. Finally, at least some of residues 195–210 must be exposed to the IMS (11). Given the number of residues available in this region, β12 and β13 are proposed to be only six residues long, the minimum needed to span the membrane (46). All or part of β14 is predicted by all algorithms (Fig. 1); a single strand (G-214 to T-223) encompasses β13 and β14 of the model of Mannella et al. (12). β14 is placed between residues E-220 and I-227, leaving P-229 in the IMS. Replacement of E-220 does not affect ion selectivity; if it resides in β14, it must be in a position that limits its contribution to ion selectivity.

The segment after β14 is of interest because it contains regions that can be deleted without preventing efficient pore

formation. 228porin and 238porin formed large pores, suggesting that residues 228–232 and 238–242 are not involved in β-strand formation. The region between these two segments is likely too short to form a transmembrane β-strand, suggesting that residues 228–242 exist in a large, IMS loop that would place R-240 on the same side of the membrane as T-135. Within this region, K-234 contributes to ion selectivity; this observation is compatible with a large loop that can enter the pore and contribute to the charge characteristics of the channel. 228porin forms a cation-selective pore, and the deleted segment includes D-228, whose absence would decrease the net negative charge in the region, and therefore would be unlikely to directly shift the ion selectivity toward cations. Therefore, residues 228–232 are not direct determinants of ion selectivity, but perhaps interact with a region of the protein that is. P-229 is also absent in 228porin, which may alter the topology of the loop that contains it, perhaps interrupting interactions responsible for gating. K-234 and K-236, which are required for the stable assembly of yeast VDAC1 into the mitochondrial outer membrane (47), are also within this proposed loop.

β15 is predicted by the lack of pore formation by 242porin. It is also required to place at least some of segment 251–268 facing the cytosol, where it would be accessible to antibody binding (11) (Fig. 1). Placing this β-strand between residues A-243 and L-250 places N-248 (K-248 in yeast) inside and R-252 outside of the membrane, as predicted in Blachly-Dyson et al. (5). β15 was not predicted by Benz (2) or Song et al. (30). β16 (V-255 to S-262) places V-255 in the membrane (5) and D-264 on the same side of the membrane as R-240. A β-strand at the position of β16 is predicted in all models (Fig. 1 and residues E-253 to D-264 in Mannella et al. (12)). A final β-strand comprised of the region containing residues 274–283 is predicted in most models (see Fig. 1), but cannot be accommodated in the current arrangement because it would create an odd number of β-strands. ΔCporin lacks residues 269–283 and forms pores in artificial bilayers (9), further supporting the absence of a β-strand in this region. In addition, an epitope between 272 and 283 is accessible in mitochondria with ruptured outer membranes, suggesting that this segment resides in the IMS. This prediction is also compatible with the fact that K-267 and K-274 do not contribute to ion selectivity. A role for E-282 (D-282 in yeast) in the process is possible if the C-terminus interacts with the channel, as may be suggested by fluorescence analysis (Fig. 3; see below). It is noteworthy that the amino and carboxyl termini of two β-barrel proteins of the outer membrane protein import machinery TOM40 (48), and Tob55/Omp85 (49) are also likely exposed to the IMS.

Overall, the revisions to β8 through β16 the model include most of the β-strand regions predicted on the basis of alternating hydrophobic and hydrophilic residues (2). The importance of this organization has recently been demonstrated; a pore was generated in an artificial membrane by the assembly of identical 24-residue peptides, which consisted of hydrophobic residues alternating with either glycine or serine (50). In terms of the other secondary structure prediction methods, it is interesting that the deletion analysis does not support all of the β-strands predicted by two neural networks ((4), and PRED-TM$\beta\beta$; see Fig. 1, *E* and *F*), both trained on bacterial porins. Possibly key features of bacterial porins, such as interfaces between subunits, and extracellular latching loops and eyelet regions, are not relevant to mitochondrial porins.

Effects of deletions on the detergent-folded state of detergent solubilized porin

The experiments presented in this study utilized mitochondrial porin that was denatured and isolated from *E. coli*. Although the wild-type protein could be renatured to a β-rich state, detergent-solubilization of the denatured form of the protein is less than optimal because it does not reflect in vivo conditions, where chaperones and lipid may contribute to folding of the native protein, and might be able to induce correct folding of some of the variants. Future studies will involve in vivo expression of these variants to determine if they are capable of folding under native conditions.

The sensitivity of the black lipid bilayer system, which detects the formation of individual pores, was revealed by the studies presented herein. For example, pore formation by 166porin and 186porin could be detected, even though it could not be stably maintained in detergent for analysis by CD or fluorescence spectroscopy. This observation suggests that rare, insertion-competent, β-barrel conformations exist in a mixture of alternative arrangements and soluble aggregates. These rare conformations usually gave rise to small pores, suggestive of barrels lacking one or more native strands. The alternative topologies formed by several of the variants likely retain structural elements near the N- and C-termini of the protein that allow formation of a complete β-barrel.

Fluorescence has not been used previously to investigate mitochondrial porins. Several variants in this study displayed altered Trp fluorescence. The deletions involved the C-terminal half of the protein, where W-209 would be most likely to be affected by alternative arrangements of the protein in detergent. In addition to detergent molecules, the adjacent strands, which might be involved in β-hairpin structures or more extensive β-sheets, could contribute to the environment surrounding the predicted β-strand containing W-209. Generally, the λ_{max} of Trp fluorescence was shifted by <5 nm. Given the ± 3 nm precision of the fluorometer, this suggests that the hydrophobicity of the environment surrounding the Trp residues was similar in the wild-type and variant proteins. With the exception of ΔCporin, the Trp fluorescence spectra of porin variants with high or intermediate levels of pore formation were similar to that of the wild-type protein, as might be the case if there were only minor differences between the folded states of the variants and His_6-porin. β12, the strand adjacent to that harboring W-209,

would include the region disrupted in 195porin (see Fig. 4). For this variant, the relative intensity of the fluorescence signal is somewhat lower (70%), whereas λ_{max}Trp is very similar to that of His_6-porin, suggesting that a quenching residue is placed in closer proximity to W-209 than it was in the wild-type porin. In contrast, fluorescence intensity of ΔCporin was about twice that of His_6-porin (Table 1). One explanation is that the C-terminus is in close proximity to one of the Trp residues in the Genapol-X80 solubilized protein, and the potential quenching residues H-273 and E-282 are absent in ΔCporin. A variety of Trp fluorescence profiles was seen for variants with low pore-forming ability. Most of the deletions in other predicted β-strands do not lead to large changes in λ_{max}Trp, indicating that the environments surrounding the two Trp residues in the variants and the wild-type protein are of similar hydrophobicity. Strong quenching is observed in 126porin, 147porin, 166porin, and 186porin. Combined with the low efficiency of pore formation by these variants, these data suggest significant changes that place one or both of the Trp residues in closer proximity to quenching moieties. Red-shifted Trp fluorescence was observed for 173porin, indicating exposure of at least one of the Trp residues to a less hydrophobic environment; large-scale alterations to the folded state are also suggested by the very low β-strand content of 173porin in Genapol X-80 and very low levels of pore formation. Nonetheless, λ_{max}Trp for this variant is still significantly blue-shifted compared to tryptophans completely exposed to the aqueous environment (Class III fluorescence, λ_{max}Trp ~ 347 nm (39)), indicating that 173porin is in a conformation in which the Trp residues are still partially buried. Remarkably, 120porin shows wild-type fluorescence and β-strand content, even though it does not form pores, emphasizing the fact that β-strand content and fluorescence properties are not predictors of pore-forming ability. The deletion in 120porin is predicted to involve two β-strands (Fig. 4), and ~30% β-strand content would be expected if ~70% of the deleted residues were involved in the formation of β-strands. Conversely, pore formation is not indicative of amenability to detergent folding; 177porin forms gated pores at low frequency, but could not be maintained in soluble form for fluorescence or CD analyses.

The porin variants described herein have provided information regarding the folded state of mitochondrial porin in detergent micelles and artificial membranes. Further studies will focus on in vitro and in vivo import competence of these variants and their interactions with components of the recently identified outer membrane import system specific to β-barrel proteins ((49), reviewed in (51)).

We gratefully acknowledge Dr. J. O'Neil, University of Manitoba, for his invaluable assistance with CD. The excellent technical assistance of Jillian Waruk is also acknowledged.

This work was supported by a Discovery Grant from the Natural Sciences and Engineering Research Council, and funds from the University of Manitoba Research Grants Program to D.A.C.; grants from the Deutsche Forschungsgemeinschaft and the Fonds der Chemischen Industrie to R.B.; and a Manitoba Health Research Graduate Fellowship to D.C.B.

REFERENCES

1. Bay, D. C., and D. A. Court. 2002. Origami in the outer membrane: the transmembrane arrangement of mitochondrial porins. *Biochem. Cell Biol.* 80:551–562.
2. Benz, R. 1994. Permeation of hydrophilic solutes through mitochondrial outer membranes: review on mitochondrial porins. *Biochim. Biophys. Acta.* 1197:167–196.
3. Rauch, G., and O. Moran. 1994. On the structure of mitochondrial porins and its homologies with bacterial porins. *Biochem. Biophys. Res. Commun.* 200:908–915.
4. Casadio, R., I. Jacoboni, A. Messina, and V. De Pinto. 2002. A 3D model of the voltage-dependent anion channel (VDAC). *FEBS Lett.* 520:1–7.
5. Blachly-Dyson, E., S. Peng, M. Colombini, and M. Forte. 1990. Selectivity changes in site-directed mutants of the VDAC ion channel: structural implications. *Science.* 247:1233–1236.
6. Song, J., C. Midson, E. Blachly-Dyson, M. Forte, and M. Colombini. 1998. The sensor regions of VDAC are translocated from within the membrane to the surface during the gating processes. *Biophys. J.* 74:2926–2944.
7. Mihara, K., and R. Sato. 1985. Molecular cloning and sequencing of cDNA for yeast porin, an outer mitochondrial membrane protein: a search for targeting signal in the primary structure. *EMBO J.* 4:769–774.
8. Kleene, R., N. Pfanner, R. Pfaller, T. A. Link, W. Sebald, W. Neupert, and M. Tropschug. 1987. Mitochondrial porin of *Neurospora crassa*: cDNA cloning, in vitro expression and import into mitochondria. *EMBO J.* 6:2627–2633.
9. Popp, B., D. A. Court, R. Benz, W. Neupert, and R. Lill. 1996. The role of the N and C termini of recombinant *Neurospora* mitochondrial porin in channel formation and voltage-dependent gating. *J. Biol. Chem.* 271:13593–13599.
10. Koppel, D. A., K. W. Kinnally, P. Masters, M. Forte, E. Blachly-Dyson, and C. A. Mannella. 1998. Bacterial expression and characterization of the mitochondrial outer membrane channel. Effects of N-terminal modifications. *J. Biol. Chem.* 273:13794–13800.
11. Stanley, S., J. A. Dias, D. D'Arcangelis, and C. A. Mannella. 1995. Peptide-specific antibodies as probes of the topography of the voltage-gated channel in the mitochondrial outer membrane of *Neurospora crassa*. *J. Biol. Chem.* 270:16694–16700.
12. Mannella, C. A., A. F. Neuwald, and C. E. Lawrence. 1996. Detection of likely transmembrane beta strand regions in sequences of mitochondrial pore proteins using the Gibbs sampler. *J. Bioenerg. Biomembr.* 28: 163–169.
13. Schulz, G. E. 2000. beta-Barrel membrane proteins. *Curr. Opin. Struct. Biol.* 10:443–447.
14. Arora, A., F. Abildgaard, J. H. Bushweller, and L. K. Tamm. 2001. Structure of outer membrane protein A transmembrane domain by NMR spectroscopy. *Nat. Struct. Biol.* 8:334–338.
15. Fernández, C., C. Hilty, S. Bonjour, K. Adeishvili, K. Pervushin, and K. Wüthrich. 2001. Solution NMR studies of the integral membrane proteins OmpX and OmpA from *Escherichia coli*. *FEBS Lett.* 504: 173–178.
16. Fernández, C., C. Hilty, G. Wider, P. Guntert, and K. Wüthrich. 2004. NMR structure of the integral membrane protein OmpX. *J. Mol. Biol.* 336:1211–1221.
17. Popp, B., S. Gebauer, K. Fischer, U. I. Flügge, and R. Benz. 1997. Study of structure and function of recombinant pea root plastid porin by biophysical methods. *Biochemistry.* 36:2844–2852.
18. Rutz, J. M., J. Liu, J. A. Lyons, J. Goranson, S. K. Armstrong, M. A. McIntosh, J. B. Feix, and P. E. Klebba. 1992. Formation of a gated

channel by a ligand-specific transport protein in the bacterial outer membrane. *Science*. 258:471–475.

19. Schulein, K., C. Andersen, and R. Benz. 1995. The deletion of 70 amino acids near the N-terminal end of the sucrose-specific porin ScrY causes its functional similarity to LamB in vivo and in vitro. *Mol. Microbiol.* 17:757–767.
20. Andersen, C., C. Bachmeyer, H. Tauber, R. Benz, J. Wang, V. Michel, S. M. Newton, M. Hofnung, and A. Charbit. 1999. In vivo and in vitro studies of major surface loop deletion mutants of the *Escherichia coli* K-12 maltoporin: contribution to maltose and maltooligosaccharide transport and binding. *Mol. Microbiol.* 32:851–867.
21. Saxena, K., V. Drosou, E. Maier, R. Benz, and B. Ludwig. 1999. Ion selectivity reversal and induction of voltage-gating by site-directed mutations in the *Paracoccus denitrificans* porin. *Biochemistry*. 38: 2206–2212.
22. Kleivdal, H., P. Puntervoll, and H. B. Jensen. 2001. Topological investigations of the FomA porin from *Fusobacterium nucleatum* and identification of the constriction loop L6. *Microbiology*. 147:1059–1067.
23. Phale, P. S., A. Philippsen, T. Kiefhaber, R. Koebnik, V. P. Phale, T. Schirmer, and J. P. Rosenbusch. 1998. Stability of trimeric OmpF porin: the contributions of the latching loop L2. *Biochemistry*. 37:15663–15670.
24. Traurig, M., and R. Misra. 1999. Identification of bacteriophage K20 binding regions of OmpF and lipopolysaccharide in *Escherichia coli* K-12. *FEMS Microbiol. Lett.* 181:101–108.
25. Langenscheid, J., H. Killmann, and V. Braun. 2004. A FhuA mutant of *Escherichia coli* is infected by phage T1-independent of TonB. *FEMS Microbiol. Lett.* 234:133–137.
26. Achouak, W., T. Heulin, and J. M. Pages. 2001. Multiple facets of bacterial porins. *FEMS Microbiol. Lett.* 199:1–7.
27. Koebnik, R. 1999. Structural and functional roles of the surface-exposed loops of the beta-barrel membrane protein OmpA from *Escherichia coli*. *J. Bacteriol.* 181:3688–3694.
28. Killmann, H., R. Benz, and V. Braun. 1993. Conversion of the FhuA transport protein into a diffusion channel through the outer membrane of *Escherichia coli*. *EMBO J.* 12:3007–3016.
29. Runke, G., E. Maier, J. D. O'Neil, R. Benz, and D. A. Court. 2000. Functional characterization of the conserved ''GLK'' motif in mitochondrial porin from *Neurospora crassa*. *J. Bioenerg. Biomembr.* 32:563–570.
30. Song, J., C. Midson, E. Blachly-Dyson, M. Forte, and M. Colombini. 1998. The topology of VDAC as probed by biotin modification. *J. Biol. Chem.* 273:24406–24413.
31. Bagos, P. G., T. D. Liakopoulos, I. C. Spyropoulos, and S. J. Hamodrakas. 2004. A web server for predicting the topology of beta-barrel outer membrane proteins. *Nucleic Acids Res.* 32:W400–W404.
32. Hanahan, D. 1983. Studies on transformation of *Escherichia coli* with plasmids. *J. Mol. Biol.* 166:557–580.
33. Bullock, W., J. Fernandez, and J. Short. 1987. XL1-Blue: a high efficiency plasmid transforming *recA Escherichia coli* strain with beta-galactosidase selection. *Biotechniques*. 5:376–379.
34. Villarejo, M. R., and I. Zabin. 1974. Beta-galactosidase from termination and deletion mutant strains. *J. Bacteriol.* 120:466–474.
35. Benz, R., K. Janko, W. Boos, and P. Lauger. 1978. Formation of large, ion-permeable membrane channels by the matrix protein (porin) of *Escherichia coli*. *Biochim. Biophys. Acta.* 511:305–319.
36. Perczel, A., K. Park, and G. D. Fasman. 1992. Analysis of the circular dichroism spectrum of proteins using the convex constraint algorithm: a practical guide. *Anal. Biochem.* 203:83–93.
37. Park, K., A. Perczel, and G. D. Fasman. 1992. Differentiation between transmembrane helices and peripheral helices by the deconvolution of circular dichroism spectra of membrane proteins. *Protein Sci.* 1:1032–1049.
38. Mao, D., E. Wachter, and B. A. Wallace. 1982. Folding of the mitochondrial proton adenosinetriphosphatase proteolipid channel in phospholipid vesicles. *Biochemistry*. 21:4960–4968.
39. Reshetnyak, Y. K., Y. Koshevnik, and E. A. Burstein. 2001. Decomposition of protein tryptophan fluorescence spectra into log-normal components. III. Correlation between fluorescence and micro-environment parameters of individual tryptophan residues. *Biophys. J.* 81:1735–1758.
40. Ladokhin, A. S. 2000. Fluorescence spectroscopy in peptide and protein analysis. *In* Encyclopedia of Analytical Chemistry. R. A. Meyers, editor. John Wiley and Sons, Chichester. 5762–5779.
41. Court, D. A., R. Kleene, W. Neupert, and R. Lill. 1996. Role of the N- and C-termini of porin in import into the outer membrane of *Neurospora* mitochondria. *FEBS Lett.* 390:73–77.
42. Zaid, H., S. Abu-Hamad, A. Israelson, I. Nathan, and V. Shoshan-Barmatz. 2005. The voltage-dependent anion channel-1 modulates apoptotic cell death. *Cell Death Differ*. 12:751–760.
43. Konstantinova, S. A., K. A. Mannella, V. P. Skulachev, and D. B. Zorov. 1994. Detection of porin in inter-mitochondrial contacts. *Biokhimiia*. 59:1109–1121.
44. Mannella, C. A. 1997. Minireview: on the structure and gating mechanism of the mitochondrial channel, VDAC. *J. Bioenerg. Biomembr*. 29:525–531.
45. Guo, X. W., and C. A. Mannella. 1993. Conformational change in the mitochondrial channel, VDAC, detected by electron cryo-microscopy. *Biophys. J.* 64:545–549.
46. Koebnik, R., K. P. Locher, and P. Van Gelder. 2000. Structure and function of bacterial outer membrane proteins: barrels in a nutshell. *Mol. Microbiol.* 37:239–253.
47. Smith, M. D., M. Petrak, P. D. Boucher, K. N. Barton, L. Carter, G. Reddy, E. Blachly-Dyson, M. Forte, J. Price, K. Verner, and others. 1995. Lysine residues at positions 234 and 236 in yeast porin are involved in its assembly into the mitochondrial outer membrane. *J. Biol. Chem.* 270:28331–28336.
48. Künkele, K. P., P. Juin, C. Pompa, F. E. Nargang, J. P. Henry, W. Neupert, R. Lill, and M. Thieffry. 1998. The isolated complex of the translocase of the outer membrane of mitochondria. Characterization of the cation-selective and voltage-gated preprotein-conducting pore. *J. Biol. Chem.* 273:31032–31039.
49. Gentle, I., K. Gabriel, P. Beech, R. Waller, and T. Lithgow. 2004. The Omp85 family of proteins is essential for outer membrane biogenesis in mitochondria and bacteria. *J. Cell Biol.* 164:19–24.
50. Thundimadathil, J., R. W. Roeske, and L. Guo. 2005. A synthetic peptide forms voltage-gated porin-like ion channels in lipid bilayer membranes. *Biochem. Biophys. Res. Commun.* 330:585–590.
51. Paschen, S. A., W. Neupert, and D. Rapaport. 2005. Biogenesis of beta-barrel membrane proteins of mitochondria. *Trends Biochem. Sci.* 30:575–582.